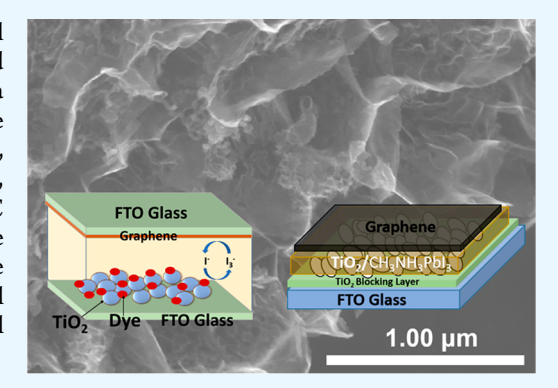
# Lithium-Chemical Synthesis of Highly Conductive 3D Mesoporous Graphene for Highly Efficient New Generation Solar Cells

Wei Wei,<sup>†</sup> Dario Stacchiola,<sup>‡®</sup> Nusnin Akter,<sup>§</sup> J. Anibal Boscoboinik,<sup>‡®</sup> and Yun Hang Hu\*<sup>,†®</sup>

Supporting Information

ABSTRACT: In this study, a highly conductive three-dimensional mesoporous graphene (3DMG), which was synthesized by our discovered reaction of lithium (Li) liquid and CO gas, was demonstrated as a promising electrode material for the hole transport material (HTM) free perovskite solar cell (PSC) and the dye-sensitized solar cell (DSSC), achieving high energy conversion efficiencies of 8.60% and 9.19%, respectively. The DSSC efficiency is higher than that (7.96%) of a DSSC with a standard Pt counter electrode. Furthermore, it was found that the electrical conductivity of 3DMG played a critical role in the PSC, but the DSSC performance was dependent on both its surface area and electrical conductivity. This would provide a novel approach to synthesize ideal electrode materials for energy devices.



KEYWORDS: 3D graphene, dye-sensitized solar cells, perovskite solar cells

arbon-based nanomaterials exhibit unique size-and structure-dependent properties. Graphene, a novel nanomaterial with a single sheet of carbon atoms packed in a hexagonal lattice, possesses fascinating properties, such as high surface area, high thermal conductivity, fast charge carrier mobility, high optical transmittance, and chemical inertness. 1-A number of production methods have been developed for the graphene synthesis, including mechanical exfoliation, 4 solution processable graphene oxide followed by chemical reduction,<sup>5</sup> epitaxial growth by thermal desorption of Si atoms from the SiC surface,6 epitaxial growth by chemical vapor deposition (CVD) on transition metals, solvothermal synthesis, and unzipping carbon nanotubes.9 Among these, Hummer's method and CVD method can not only produce twodimensional but also three-dimensional graphene. Furthermore, the assembled 3D graphene materials can provide inherently excellent properties of 2D graphene sheets (such as high electronic, optical, and catalytic properties) and exhibit large specific surface area, strong mechanical strength, high electron conductivity, and fast mass transport kinetics. However, those techniques are suffering some significant drawbacks. The Hummer method exploits toxic/hazardous chemicals for the reduction of graphene oxide (GO) to graphene. Furthermore, the presence of too many defects in graphene synthesized with the Hummer approach decrease its conductivity. 11 For the CVD method, its high energy and material costs and complicated operational conditions limit its practical applications. 12 In the past few years, we successfully

synthesized various 3D graphene with controllable shape via our discovered reactions. The 3D graphene possesses high electrical conductivities and large surface areas, constituting promising excellent properties for energy devices. Very recently, we found an efficient approach to prepare highly dense porous carbon nanomaterials via an undiscovered reaction between Li and CO.19 Furthermore, the novel materials exhibited excellent performance for supercapacitors. 19 In this work, we extended this success to produce 3D mesoporous graphene (3DMG) for new generation solar cells, dye-sensitized solar cells (DSSCs), and HTM-free perovskite solar cells (PSCs):

$$2\text{Li}_{(l)} + \text{CO}_{(g)} \rightarrow \text{C}_{(s)} + \text{Li}_2\text{O}_{(s)}$$
 (1)

$$\text{Li}_2\text{O}_{(s)} + 2\text{CO}_{(g)} \rightarrow \text{C}_{(s)} + \text{Li}_2\text{CO}_{3(s)}$$
 (2)

The reaction between Li and CO (eqs 1 and 2) was employed to synthesize 3D mesoporous graphene (3DMG) for the following reasons. The Gibbs free energy and enthalpy of the Li-CO reaction are negative, indicating its thermodynamically favorable and exothermic features, respectively (Figure 1A). Simultaneously formed Li<sub>2</sub>CO<sub>3</sub> can play two roles: (1) isolating graphene sheets from each other and thus preventing the formation of graphite and (2) controlling the shape of

Received: November 19, 2018 Accepted: January 24, 2019 Published: January 24, 2019



<sup>&</sup>lt;sup>†</sup>Department of Materials Science and Engineering, Michigan Technological University, 1400 Townsend Dr., Houghton, Michigan 49931, United States

<sup>&</sup>lt;sup>‡</sup>Center for Functional Nanomaterials, Brookhaven National Laboratory, Upton, New York 11973, United States

 $<sup>^{\$}</sup>$ Department of Materials Science and Chemical Engineering, Stony Book University, Stony Brook, New York 11790, United States

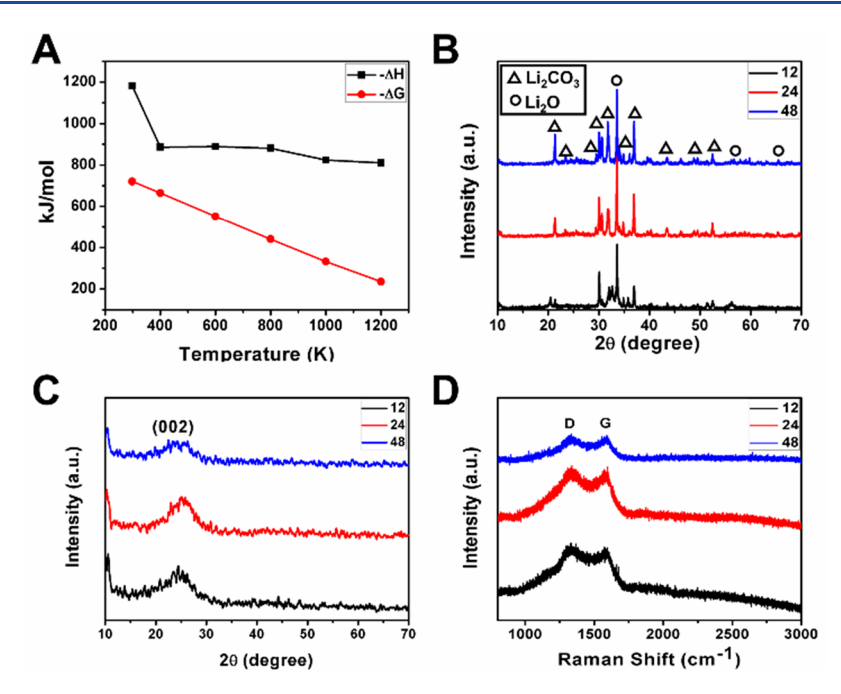


Figure 1. (A) Gibbs free energy and enthalpy of Li–CO reaction versus temperature. (B) XRD patterns of solid products from the reaction. (C) XRD patterns of the carbon material obtained by treating the solid products with HCl. (D) Raman spectrum of the carbon material obtained by treating the solid products with HCl.

graphene as a template. With this strategy, 3D mesoporous graphene (3DMG) was synthesized and demonstrated as excellent electrode material for DSSCs and PSCs as follows.

Lithium (Li) particles (0.1 mol; from Aldrich) reacted with CO in a batch ceramic-tube reactor at an initial pressure of 50 psi, and the temperature was raised from room temperature to 600 °C by 10 °C/min and then kept at the target temperature for 12, 24, or 48 h. In order to further confirm the reaction, the products were subjected to X-ray diffraction (XRD) measurements. As shown in Figure 1B, diffraction peaks for Li<sub>2</sub>CO<sub>3</sub> can be observed, confirming the proposed reaction. Li<sub>2</sub>CO<sub>3</sub> was then removed by hydrochloric acid treatment. The remained products were washed with H<sub>2</sub>O for more than ten times and dried in an oven overnight. The obtained black powder was identified as carbon with oxygen functional groups by elemental analysis (Table 1). The XRD patterns of the carbon

Table 1. Element Analysis and EDS Analysis of Graphene Sheets

sample	element analysis		EDS		
	C (%)	O (%)	C (%)	O (%)	
3DMG-12	91.23	8.77	94.18	5.82	
3DMG-24	91.74	8.26	96.75	3.25	
3DMG-48	92.81	7.19	96.93	3.07	

presents a diffraction peak at  $2\theta = 25.9^{\circ}$ , which can be indexed to the (002) plane of the graphitic structure of carbon. Furthermore, the average interlayer space of the material is 3.55 Å, which is larger than the interlayer space of graphite. The oxygen functional groups reveal that this material possesses a rich defect feature, which can be evaluated by Raman spectra. The major natures, commonly observed in graphene, are the D band at approximately 1350 cm<sup>-1</sup> and G band at 1580 cm<sup>-1</sup>. The D peak ultimately gives a relative measure of the amount of sp<sup>3</sup> carbons in the surrounding area

and the G band corresponds to graphite-like sp<sup>2</sup> carbon. Defects (such as impurity atoms, functional groups, heptagon—hexagon pairs, folding, etc.) of the graphene layers give rise to the D band. As shown in Figure 1D, the Raman spectrum exhibits a clear G peak, providing evidence of a sp<sup>2</sup> bonded carbon. A strong D peak was also observed, indicating that the graphene sheets have a high density of defects. Surface defects are formed due to the presence of oxygenated functional groups.

A field emission scanning electron microscope (FESEM) was employed to evaluate the nanostructure of graphene sheets. As shown in Figure 2A-C, the graphene sheets constitute a three-dimensional porous frameworks with curved graphene sheets connected with each other. The thickness of one sheet is about 2 nm, which indicates that one layer consists of 6 graphene sheets. The samples were denoted as 3DMG-12, 3DMG-24, and 3DMG-48 for materials synthesized for 12, 24, and 48 h, respectively. Figure 2D shows the C 1s X-ray photoelectron spectroscopy (XPS) for 3DMG. The deconvolution of the C 1s peak revealed four components centered at 284.6, 286.4, 288.3, and 290.4 eV, which would be associated with C-C, C-O, C=O, and O-C=O. This is consistent with Raman results. The surface area and pore structure of 3DMG materials were measured by N<sub>2</sub> adsorption at liquid nitrogen temperature. Figure 3A shows a type V isotherm with a type H1 hysteresis loop, indicating that the graphene sheets possess mesopores. The specific surface areas, which were calculated with the BET model, are approximately 525, 625, and 324 m<sup>2</sup> g<sup>-1</sup> for 3DMG-12, 3DMG-24, and 3DMG-48, respectively. The pore size distributions were calculated with the BJH model, showing a range of 1-210 nm as shown in Figure 3B. The average pore size diameter for 3DMG-12, 3DMG-24, and 3DMG-48 are 9.8, 9.9, and 14.1 nm, respectively. This indicates that the graphene possesses mesopores, which should make it easier for transporting electrolyte ions and filling of precursors. Moreover, the sheet

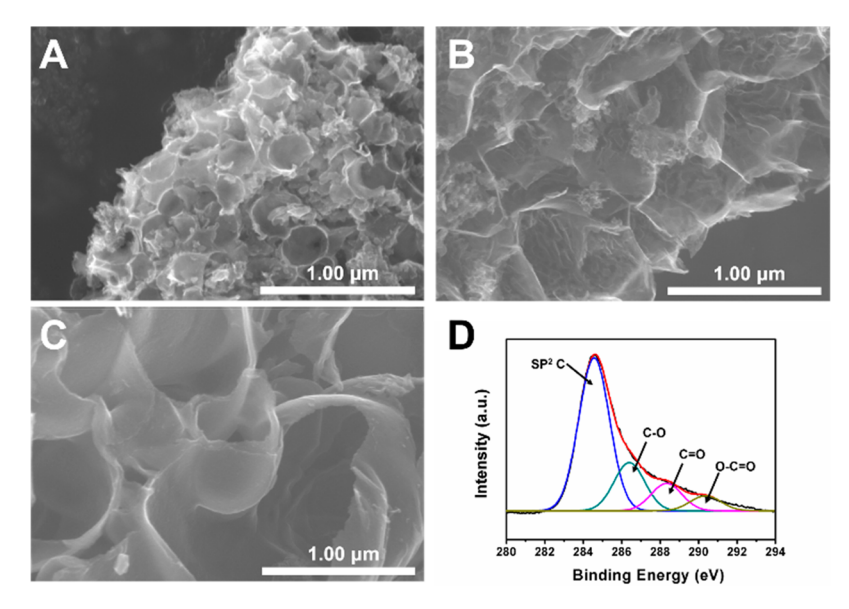


Figure 2. FESEM images of graphene sheets obtained with reaction times of (A) 12 h, (B) 24 h, and (C) 48 h. (D) XPS spectrum of graphene sheets obtained with reaction times of 48 h.

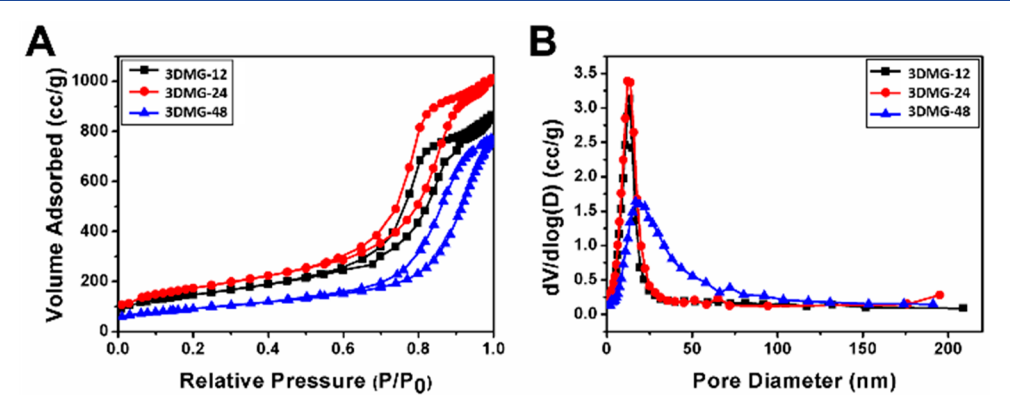


Figure 3. (A) Adsorption/desorption curves of graphene sheets. (B) Pore size distribution of graphene sheets.

resistances of the films with 3DMG-12, 3DMG-24, and 3DMG-48 were also measured by four-point probe analysis, and they are 1641.1, 987.2, and 478.3  $\Omega$  sq $^{-1}$ , respectively. The structural defects and the high conductivity of graphene offer unique opportunities for its applications related to energy conversion and storage.

To deal with the global energy challenge and environmental crisis, one of the most promising technologies in the field of electrochemical energy storage and conversion is the conversion of sustainable and clean solar energy directly into electricity using photovoltaic devices. Owing to their low cost, relatively high conversion efficiency, and simple fabrication process, dye-sensitized solar cells (DSSCs) have attracted extensive attention and have been considered as one of the most prospective alternatives to traditional Si solar cells.<sup>20-24</sup> A typical DSSC holds a sandwich structure with a dyesensitized nanocrystalline photoanode, an electrolyte containing I<sup>-</sup>/I<sub>3</sub><sup>-</sup> redox couple, and a catalytic counter electrode. As one of the main components of DSSCs, the counter electrode plays a significant role in regulating the photovoltaic performance of the cell by collecting the electrons from external circuit and catalyzing the I3- reduction at the electrolyte/counter electrode interface. Thus, an ideal counter electrode should exhibit good electrocatalytic activity and

electrical conductivity. So far, Pt is still the preferred counter electrode material in DSSCs due to its excellent electrocatalytic activity, high conductivity, and good stability. 25-29 However, the limited reserves and associated high cost of Pt severely restrict its large-scale application in DSSCs. Therefore, considerable efforts have been made to replace Pt counter electrode with cheaper materials, such as carbonaceous materials, <sup>30–32</sup> conducting polymer, <sup>33,34</sup> transition-metal compounds, <sup>16,35–41</sup> and metal alloy. <sup>42,43</sup> Herein, the obtained 3DMG was explored as counter electrode material for DSSCs as follows. The photoelectrode of the DSSCs is N719 dyesensitized TiO<sub>2</sub> film on a fluorine-doped tin oxide (FTO) glass plate, and the electrolyte is a I<sub>3</sub><sup>-</sup>/I<sup>-</sup>-based liquid. Figure 4A shows the characteristic I-V curves of the DSSCs using different reaction times with graphene as the counter electrodes. The detailed photovoltaic parameters of the DSSCs from I-V curves are summarized in Table 2. The DSSC with 3DMG-12 CE showed comparable efficiency with that of Pt CE (Figure S1 in the Supporting Information). The DSSC with 3DMG-24 CE exhibited the best performance with the short-circuit current density  $(I_{sc})$  of 17.75 mA cm<sup>-2</sup>, opencircuit voltage  $(V_{oc})$  of 0.77 V, fill factor (FF) of 0.67, and power conversion efficiency ( $\eta$ ) of 9.19% under illumination of AM1.5 simulated sunlight with a power density of 100 mW

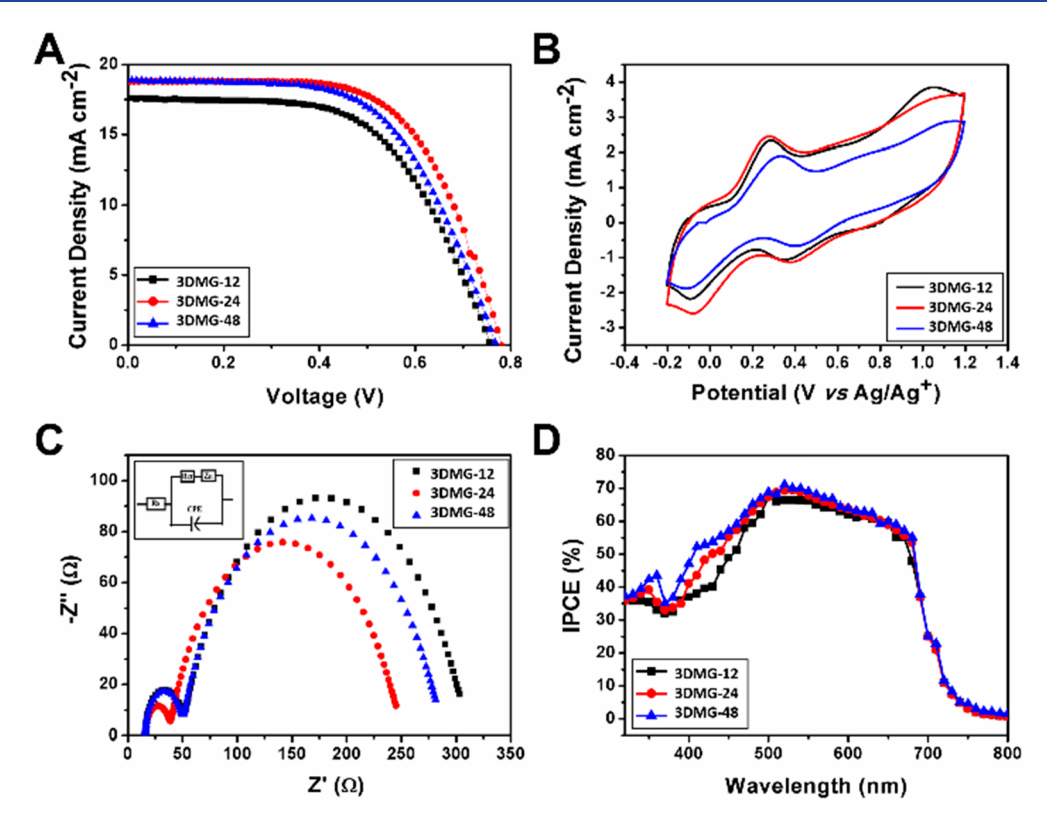


Figure 4. Characterization of DSSCs: (A) I-V curves, (B) CV curves, (C) EIS spectrum, and (D) IPCE spectrum.

Table 2. Photovoltaic Performance of Graphene Sheets in DSSCs

CE	$(\mathrm{mA~cm}^{I_{\mathrm{sc}}})$	$V_{ m oc} \ ( m V)$	FF	η (%)	$\stackrel{R_{_{ m S}}}{(\Omega)}$	$egin{aligned} R_{ m ct} \ (\Omega) \end{aligned}$	$Z_{ m N} \ (\Omega)$
3DMG- 12	17.55	0.76	0.58	7.80	16	34	256
3DMG- 24	17.75	0.77	0.67	9.19	16	22	208
3DMG- 48	18.90	0.76	0.60	8.56	16	33	234

cm<sup>-2</sup> in the range of 320-1100 nm. The two critical factors (electrical conductivity and catalytic activity) determine CE performance for DSSCs, namely, the larger the conductivity and the catalytic activity are, the higher the energy conversion efficiency is. When the graphene synthesis time increased from 12 to 24 h, the conductivity increased (which is reflected by a decrease in its sheet resistance), whereas the efficiency of graphene-based DSSC increased. However, when the graphene synthesis time increased to 48 h, the conductivity increased and the efficiency decreased. This indicates that the decrease in efficiency with increasing graphene synthesis time is not only due to the variation of graphene conductivity but also relates to the decreasing catalytic activity, which is reflected by a decrease in its surface area. On the other hand, 3DMG-24 processes the largest surface area, which indicates that abundant catalytic sites are exposed to the electrolyte. So, specific surface area, in other words the catalytic activity, of graphene nanosheets should be considered as another crucial factor when applied as the CE materials in DSSCs.

Cyclic voltammetry (CV) measurements were first used to demonstrate the catalytic activity of the counter electrodes. CV curves were obtained for three graphene CEs, which show two pairs of oxidation and reduction peaks. Since a DSSC CE mainly catalyzes the reduction of  $I_3^-$  to  $I^-$ , it can be evaluated by the peak current density and the peak-to-peak separation  $(E_{\rm pp})$  of  $A_{\rm ox}$  and  $A_{\rm red}$  peaks, namely, the higher the peak current density and the lower the  $E_{\rm pp}$  value are, the better the catalytic activity is. As shown in Figure 4B, 3DMG-24 CE shows the highest peak current density and lowest  $E_{\rm pp}$  of the three electrodes, indicating it has the best electrocatalytic activity. This further supports the results of I-V measurements.

Electrochemical impedance spectroscopy (EIS) is widely applied in the investigation of the electrochemical behavior of the DSSCs. Figure 4C shows the Nyquist plots of the corresponding solar cells. Two semicircles were observed in the frequency range of 0.1-100 kHz for all samples. The different resistance contributions of each electrode were obtained by fitting the Nyquist plots to the equivalent circuit (inset) and electrochemical parameters are listed in Table 2. The intercept of the first semicircle represents the ohmic serial resistance  $(R_s)$  related to the intrinsic resistance of assembled cells. The first semicircle corresponds to charge-transfer resistance  $(R_{ct})$  at the CE/electrolyte interface, which changes inversely with catalytic ability of CEs for the reduction of I<sub>3</sub><sup>-</sup> to I-, while the semicircle in the lower frequency region is attributed to the Nernst diffusion process  $(Z_N)$  of the triiodid/ iodide couple; a low Nernst diffusion impedance suggests a fast ion diffusion process. As the graphene counter electrodes have nearly the same value of  $R_s$ , the effect of  $R_s$  on photovoltaic performance can be neglected, whereas  $Z_N$  values of 3DMG-24 are much smaller than those of the other samples, indicating its very fast ion diffusion in the electrolyte. The value of  $R_{ct}$  is inverse to the order of electrocatalytic activity. Therefore, sample 3DMG-24 has the best electrocatalytic activity because of its lowest R<sub>ct</sub>. Furthermore, incident photon-to-current conversion efficiency (IPCE) curves further support the results of I-V measurements (Figure 4D).

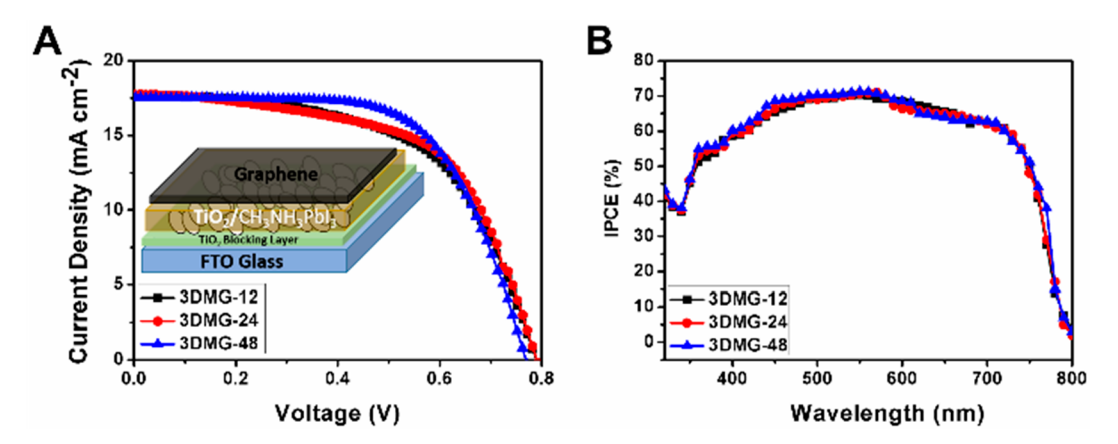


Figure 5. Characterization of PSCs: (A) I-V curves with device configuration inset and (B) IPCE spectrum.

Perovskite solar cells (PSCs) have received intensive research interests over the past few years because of their rapid power conversion efficiency (PCE) growth, with the latest record over 22%. The low cost and relatively simpler fabrication processes of PSC, as well as ease of achieving high PCEs which can match with that of the silicon cells, make it a promising and competitive solar cell technology. However, the commonly used organic hole transport materials (HTMs), like small organic molecular (Spiro-OMeTAD) or organic polymers (P3HT, PEDOT/PSS, or PTAA), are expensive and might lead to severe instability problems. The universally used counter electrode materials such as Au or Ag require a high vacuum for thermal evaporation process, which further increases the cost of fabrication of PSCs. In order to overcome these disadvantages that hinder the industrialization of PSCs, HTM free perovskite solar cells have been proposed. 49-51 In particular, carbonbased HTM-free PSCs show much promise to solve the problems mentioned above because carbon materials are earth abundant, low-cost, and environmentally stable. This stimulated us to explore the synthesized 3DMG as counter electrode materials for HTM-free perovskite solar cells due to their high electrical conductivity as follows.

To start with a compact layer, 0.15 M titanium diisopropoxide bis(acetylacetonate) was spin coated on FTO glass, followed by heat treatment at 500 °C for 30 min. Then, the perovskite layer was deposited with a two-step method, followed by doctor blade coating the 3DMG counter electrodes (Supporting Information). Figure S2 is the corresponding band structure of the device, which indicates that the 3DMG is favorable to hole transfer at the CH<sub>3</sub>NH<sub>3</sub>PbI<sub>3</sub>/3DMG interface. As shown in Figure 5A, one can see the current density (I)-voltage (V) characteristics of the HTM-free TiO<sub>2</sub>/CH<sub>3</sub>NH<sub>3</sub>PbI<sub>3</sub>/3DMG cells, in which a HTM layer was eliminated and a novel metal electrode was replaced by the inexpensive 3DMG to significantly reduce the PSC cost. The photovoltaic properties were measured under standard AM 1.5G illumination (100 mW cm<sup>-2</sup>). The values of short-circuit photocurrent  $(I_{sc})$ , open-circuit voltage  $(V_{oc})$ , fill factor (FF), and power conversion efficiency ( $\eta$ ) are listed in Table 3. The efficiency increased with increasing synthesis time of 3DMG and reached the maximum value of 8.60% with 3DMG-48. This can be attributed to the enhanced electrical conductivity of 3DMG due to the increase in its synthesis time. This is different from the DSSC, the performance of which is dependent on both the electrical conductivity and the surface

Table 3. Photovoltaic Performance of Graphene Sheets in PSCs

scan direction	$I_{\rm sc}~({\rm mA~cm}^{-2})$	$V_{\rm oc}$ (V)	FF	η (%)
forward	18.00	0.78	0.58	8.18
reverse	17.52	0.77	0.64	8.60

area of 3DMG. This is because the internal surface area can be accessed by ions of electrolyte liquid in a DSSC, but it may not be used in a PSC (due to the contact between solid particles of  ${\rm TiO_2}$  and 3DMG without liquid ions). The incident-photon-to-current conversion efficiency (IPCE) spectra of the PSC are presented in Figure 5B, which shows a strong spectral response in the range of 350–750 nm. The integrated current over the whole spectral response region is in good agreement with the measured  $I_{\rm SC}$  values obtained from the I–V curves.

In summary, our discovered reaction of Li and CO was successfully employed to synthesize 3D mesoporous graphene (3DMG) with high conductivity and large surface area. Furthermore, the 3DMG was demonstrated as an excellent electrode material for the hole transport material (HTM) free perovskite solar cell (PSC) and the dye-sensitized solar cell (DSSC). The PSC and the DSSC with 3DMG counter electrode exhibited high efficiencies of 8.60% and 9.19%, respectively. Furthermore, it was revealed that the PSC performance is mainly dependent on the electrical conductivity of 3DMG, but the DSSC efficiency is determined by both its electrical conductivity and surface area.

## ASSOCIATED CONTENT

## **S** Supporting Information

The Supporting Information is available free of charge on the ACS Publications website at DOI: 10.1021/acsaem.8b02014.

Full experimental details and DSSC performance with the Pt counter electrode (PDF)

## AUTHOR INFORMATION

# **Corresponding Author**

\*E-mail: yunhangh@mtu.edu.

#### ORCID ®

Dario Stacchiola: 0000-0001-5494-3205 J. Anibal Boscoboinik: 0000-0002-5090-7079 Yun Hang Hu: 0000-0002-5358-8667

Notes

The authors declare no competing financial interest.

## ACKNOWLEDGMENTS

This work was partially supported by the U.S. National Science Foundation (CBET-0931587 and CMMI-1661699). The authors also thank Charles and Carroll McArthur for their great support.

## REFERENCES

- (1) Zhu, Y.; Murali, S.; Cai, W.; Li, X.; Suk, J. W.; Potts, J. R.; Ruoff, R. S. Graphene and Graphene Oxide: Synthesis, Properties, and Applications. Adv. Mater. 2010, 22, 3906-3924.
- (2) Novoselov, K. S.; Geim, A. K.; Morozov, S. V.; Jiang, D.; Zhang, Y.; Dubonos, S. V.; Grigorieva, I. V.; Firsov, A. A. Electric Field Effect in Atomically Thin Carbon Films. Science 2004, 306, 666-669.
- (3) Geim, A. K.; Novoselov, K. S. The Rise of Graphene. Nat. Mater. 2007, 6, 183-191.
- (4) Yi, M.; Shen, Z. A Review on Mechanical Exfoliation for the Scalable Production of Graphene. J. Mater. Chem. A 2015, 3, 11700-
- (5) Marcano, D. C.; Kosynkin, D. V.; Berlin, J. M.; Sinitskii, A.; Sun, Z.; Slesarev, A.; Alemany, L. B.; Lu, W.; Tour, J. M. Improved Synthesis of Graphene Oxide. ACS Nano 2010, 4, 4806-4814.
- (6) Kim, K. S.; Zhao, Y.; Jang, H.; Lee, S. Y.; Kim, J. M.; Kim, K. S.; Ahn, J.-H.; Kim, P.; Choi, J.-Y.; Hong, B. H. Large-Scale Pattern Growth of Graphene Films for Stretchable Transparent Electrodes. Nature 2009, 457, 706-710.
- (7) Chen, X.; Zhang, L.; Chen, S. Large Area Cvd Growth of Graphene. Synth. Met. 2015, 210, 95-108.
- (8) Choucair, M.; Thordarson, P.; Stride, J. A. Gram-Scale Production of Graphene Based on Solvothermal Synthesis and Sonication. Nat. Nanotechnol. 2009, 4, 30-33.
- (9) Taghioskoui, M. Trends in Graphene Research. Mater. Today 2009, 12, 34-37.
- (10) Nardecchia, S.; Carriazo, D.; Ferrer, M. L.; Gutiérrez, M. C.; Del Monte, F. Three Dimensional Macroporous Architectures and Aerogels Built of Carbon Nanotubes and/or Graphene: Synthesis and Applications. Chem. Soc. Rev. 2013, 42, 794-830.
- (11) Jiangying, Q.; Feng, G.; Quan, Z.; Zhiyu, W.; Han, H.; Beibei, L.; Wubo, W.; Xuzhen, W.; Jieshan, Q. Highly Atom-Economic Synthesis of Graphene/Mn<sub>3</sub>O<sub>4</sub> Hybrid Composites for Electrochemical Supercapacitors. Nanoscale 2013, 5, 2999-3005.
- (12) Li, X.; Colombo, L.; Ruoff, R. S. Synthesis of Graphene Films on Copper Foils by Chemical Vapor Deposition. Adv. Mater. 2016,
- (13) Wei, W.; Chang, L.; Sun, K.; Pak, A. J.; Paek, E.; Hwang, G. S.; Hu, Y. H. The Bright Future for Electrode Materials of Energy Devices: Highly Conductive Porous Na-Embedded Carbon. Nano Lett. 2016, 16, 8029-8033.
- (14) Wei, W.; Hu, B.; Jin, F.; Jing, Z.; Li, Y.; Garcia-Blanco, A.; Stacchiola, D.; Hu, Y. H. Potassium-Chemical Synthesis of 3D Graphene from CO2 and Its Excellent Performance for HTM-Free Perovskite Solar Cells. J. Mater. Chem. A 2017, 5, 7749-7752.
- (15) Wei, W.; Sun, K.; Hu, Y. H. Synthesis of 3D Cauliflower-Fungus-Like Graphene from CO2 as a Highly Efficient Counter Electrode Material for Dye-Sensitized Solar Cells. J. Mater. Chem. A 2014, 2, 16842-16846.
- (16) Wei, W.; Sun, K.; Hu, Y. H. Direct Conversion of CO<sub>2</sub> to 3D Graphene and Its Excellent Performance for Dye-Sensitized Solar Cells with 10% Efficiency. J. Mater. Chem. A 2016, 4, 12054-12057.
- (17) Wei, W.; Sun, K.; Hu, Y. H. Synthesis of Mesochannel Carbon Nanowall Material from CO2 and Its Excellent Performance for Perovskite Solar Cells. Ind. Eng. Chem. Res. 2017, 56, 1803-1809.
- (18) Wei, W.; Hu, Y. H. Synthesis of Carbon Nanomaterials for Dye-Sensitized Solar Cells. Int. J. Energy Res. 2015, 39, 842-850.
- (19) Chang, L.; Sun, K.; Hu, Y. H. New Chemistry for New Material: Highly Dense Mesoporous Carbon Electrode for Supercapacitors with High Areal Capacitance. ACS Appl. Mater. Interfaces 2018, 10, 33162-33169.

- (20) O'Regan, B.; Gratzel, M. A Low-Cost, High-Efficiency Solar-Cell Based on Dye-Sensitized Colloidal TiO2 Films. Nature 1991, 353, 737-740.
- (21) Hagfeldt, A.; Boschloo, G.; Sun, L. C.; Kloo, L.; Pettersson, H. Dye-Sensitized Solar Cells. Chem. Rev. 2010, 110, 6595-6663.
- (22) Mathew, S.; Yella, A.; Gao, P.; Humphry-Baker, R.; Curchod, B. F. E.; Ashari-Astani, N.; Tavernelli, I.; Rothlisberger, U.; Nazeeruddin, M. K.; Gratzel, M. Dye-Sensitized Solar Cells with 13% Efficiency Achieved through the Molecular Engineering of Porphyrin Sensitizers. Nat. Chem. 2014, 6, 242-247.
- (23) Meng, X.; Yu, C.; Song, X.; Iocozzia, J.; Hong, J.; Rager, M.; Jin, H.; Wang, S.; Huang, L.; Qiu, J.; Lin, Z. Scrutinizing Defects and Defect Density of Selenium-Doped Graphene for High-Efficiency Triiodide Reduction in Dye-Sensitized Solar Cells. Angew. Chem., Int. Ed. 2018, 57, 4682-4686.
- (24) Meng, X.; Yu, C.; Zhang, X.; Huang, L.; Rager, M.; Hong, J.; Qiu, J.; Lin, Z. Active Sites-Enriched Carbon Matrix Enables Efficient Triiodide Reduction in Dye-Sensitized Solar Cells: An Understanding of the Active Centers. Nano Energy 2018, 54, 138-147.
- (25) Dao, V. D.; Choi, H. S. Pt Nanourchins as Efficient and Robust Counter Electrode Materials for Dye-Sensitized Solar Cells. ACS Appl. Mater. Interfaces 2016, 8, 1004-1010.
- (26) Fu, N. Q.; Fang, Y. Y.; Duan, Y. D.; Zhou, X. W.; Xiao, X. R.; Lin, Y. High-Performance Plastic Platinized Counter Electrode Via Photoplatinization Technique for Flexible Dye-Sensitized Solar Cells. ACS Nano 2012, 6, 9596-9605.
- (27) Lin, C. A.; Lee, C. P.; Ho, S. T.; Wei, T. C.; Chi, Y. W.; Huang, K. P.; He, J. H. Nitrogen-Doped Graphene/Platinum Counter Electrodes for Dye-Sensitized Solar Cells. ACS Photonics 2014, 1,
- (28) Aboagye, A.; Elbohy, H.; Kelkar, A. D.; Qiao, Q.; Zai, J.; Qian, X.; Zhang, L. Electrospun Carbon Nanofibers with Surface-Attached Platinum Nanoparticles as Cost-Effective and Efficient Counter Electrode for Dye-Sensitized Solar Cells. Nano Energy 2015, 11, 550-556.
- (29) Zhu, Y.; Gao, C.; Han, Q.; Wang, Z.; Wang, Y.; Zheng, H.; Wu, M. Large-Scale High-Efficiency Dye-Sensitized Solar Cells Based on a Pt/Carbon Spheres Composite Catalyst as a Flexible Counter Electrode. J. Catal. 2017, 346, 62-69.
- (30) Zhou, Z.; Sigdel, S.; Gong, J.; Vaagensmith, B.; Elbohy, H.; Yang, H.; Krishnan, S.; Wu, X. F.; Qiao, Q. Graphene-Beaded Carbon Nanofibers with Incorporated Ni Nanoparticles as Efficient Counter-Electrode for Dye-Sensitized Solar Cells. Nano Energy 2016, 22, 558-
- (31) Wang, G.; Zhang, J.; Hou, S.; Zhang, W.; Zhao, Z. Edge-Nitrogenated Graphene Nanoplatelets as High-Efficiency Counter Electrodes for Dye-Sensitized Solar Cells. Nanoscale 2016, 8, 9676-
- (32) Zheng, X.; Wei, Z.; Chen, H.; Zhang, Q.; He, H.; Xiao, S.; Fan, Z.; Wong, K. S.; Yang, S. Designing Nanobowl Arrays of Mesoporous TiO2 as an Alternative Electron Transporting Layer for Carbon Cathode-Based Perovskite Solar Cells. Nanoscale 2016, 8, 6393-6402.
- (33) Kim, D. H.; Atanasov, S. E.; Lemaire, P.; Lee, K.; Parsons, G. N. Platinum-Free Cathode for Dye-Sensitized Solar Cells Using Poly-(3,4-Ethylenedioxythiophene) (PEDOT) Formed Via Oxidative Molecular Layer Deposition. ACS Appl. Mater. Interfaces 2015, 7,
- (34) Wei, W.; Wang, H.; Hu, Y. A Review on PEDOT-Based Counter Electrodes for Dye-Sensitized Solar Cells. Int. J. Energy Res. **2014**, 38, 1099-1111.
- (35) Meng, X.; Yu, C.; Lu, B.; Yang, J.; Qiu, J. Dual Integration System Endowing Two-Dimensional Titanium Disulfide with Enhanced Triiodide Reduction Performance in Dye-Sensitized Solar Cells. Nano Energy 2016, 22, 59-69.
- (36) Wang, X.; Batter, B.; Xie, Y.; Pan, K.; Liao, Y.; Lv, C.; Li, M.; Sui, S.; Fu, H. Highly Crystalline, Small Sized, Monodisperse A-Nis Nanocrystal Ink as an Efficient Counter Electrode for Dye-Sensitized Solar Cells. J. Mater. Chem. A 2015, 3, 15905-15912.

- (37) Wei, W.; Hu, Y. H. 3D MoS<sub>2</sub>/Graphene Hybrid Layer Materials as Counter Electrodes for Dye-Sensitized Solar Cells. *Catalysis* **2016**, 28, 268–280.
- (38) Wei, W.; Sun, K.; Hu, Y. H. An Efficient Counter Electrode Material for Dyesensitized Solar Cells-Flower-Structured 1T Metallic Phase MoS<sub>2</sub>. *J. Mater. Chem. A* **2016**, *4*, 12398–12401.
- (39) Wei, W.; Wang, H.; Hu, Y. H. Unusual Particle-Size-Induced Promoter-to-Poison Transition of ZrN in Counter Electrodes for Dye-Sensitized Solar Cells. *J. Mater. Chem. A* **2013**, *1*, 14350–14357.
- (40) Wang, H.; Wei, W.; Hu, Y. H. Efficient ZnO-Based Counter Electrodes for Dye-Sensitized Solar Cells. *J. Mater. Chem. A* **2013**, *1*, 6622–6628.
- (41) Wang, H.; Wei, W.; Hu, Y. H. NiO as an Efficient Counter Electrode Catalyst for Dye-Sensitized Solar Cells. *Top. Catal.* **2014**, 57, 607–611.
- (42) Chen, X.; Tang, Q.; He, B.; Lin, L.; Yu, L. Platinum-Free Binary Co-Ni Alloy Counter Electrodes for Efficient Dye-Sensitized Solar Cells. *Angew. Chem., Int. Ed.* **2014**, *53*, 10799–10803.
- (43) Zheng, X.; Deng, J.; Wang, N.; Deng, D.; Zhang, W. H.; Bao, X.; Li, C. Podlike N-Doped Carbon Nanotubes Encapsulating Feni Alloy Nanoparticles: High-Performance Counter Electrode Materials for Dye-Sensitized Solar Cells. *Angew. Chem., Int. Ed.* **2014**, *53*, 7023–7027.
- (44) Yi, C.; Li, X.; Luo, J.; Zakeeruddin, S. M.; Grätzel, M. Perovskite Photovoltaics with Outstanding Performance Produced by Chemical Conversion of Bilayer Mesostructured Lead Halide/TiO<sub>2</sub> Films. *Adv. Mater.* **2016**, *28*, 2964–2970.
- (45) Jeon, N. J.; Noh, J. H.; Yang, W. S.; Kim, Y. C.; Ryu, S.; Seo, J.; Seok, S. I. Compositional Engineering of Perovskite Materials for High-Performance Solar Cells. *Nature* **2015**, *517*, 476–480.
- (46) Yang, W. S.; Noh, J. H.; Jeon, N. J.; Kim, Y. C.; Ryu, S.; Seo, J.; Seok, S. I. High-Performance Photovoltaic Perovskite Layers Fabricated through Intramolecular Exchange. *Science* **2015**, 348, 1234–1237.
- (47) Meng, X.; Cui, X.; Rager, M.; Zhang, S.; Wang, Z.; Yu, J.; Harn, Y. W.; Kang, Z.; Wagner, B. K.; Liu, Y.; Yu, C.; Qiu, J.; Lin, Z. Cascade Charge Transfer Enabled by Incorporating Edge-Enriched Graphene Nanoribbons for Mesostructured Perovskite Solar Cells with Enhanced Performance. *Nano Energy* **2018**, *52*, 123–133.
- (48) Ye, M.; He, C.; Iocozzia, J.; Liu, X.; Cui, X.; Meng, X.; Rager, M.; Hong, X.; Liu, X.; Lin, Z. Recent Advances in Interfacial Engineering of Perovskite Solar Cells. J. Phys. D: Appl. Phys. 2017, 50, 373002.
- (49) Mei, A.; Li, X.; Liu, L.; Ku, Z.; Liu, T.; Rong, Y.; Xu, M.; Hu, M.; Chen, J.; Yang, Y.; Grätzel, M.; Han, H. A Hole-Conductor-Free, Fully Printable Mesoscopic Perovskite Solar Cell with High Stability. *Science* **2014**, 345, 295–298.
- (50) Chen, J.; Xiong, Y.; Rong, Y.; Mei, A.; Sheng, Y.; Jiang, P.; Hu, Y.; Li, X.; Han, H. Solvent Effect on the Hole-Conductor-Free Fully Printable Perovskite Solar Cells. *Nano Energy* **2016**, *27*, 130–137.
- (51) Chen, H.; Wei, Z.; He, H.; Zheng, X.; Wong, K. S.; Yang, S. Solvent Engineering Boosts the Efficiency of Paintable Carbon-Based Perovskite Solar Cells to Beyond 14%. *Adv. Energy Mater.* **2016**, *6*, 1502087.